



**HAL**  
open science

## Identification of organic molecules with a laboratory prototype based on the Laser Ablation-CosmOrbitrap

Laura Selliez, Christelle Briois, Nathalie Carrasco, Laurent Thirkell, R. Thissen, M. Ito, R. Orthous-Daunay, Gilles Chalumeau, Fabrice Colin, Hervé Cottin, et al.

### ► To cite this version:

Laura Selliez, Christelle Briois, Nathalie Carrasco, Laurent Thirkell, R. Thissen, et al.. Identification of organic molecules with a laboratory prototype based on the Laser Ablation-CosmOrbitrap. *Planetary and Space Science*, 2019, 170, pp.42-51. 10.1016/j.pss.2019.03.003 . insu-02069251

**HAL Id: insu-02069251**

**<https://insu.hal.science/insu-02069251>**

Submitted on 15 Mar 2019

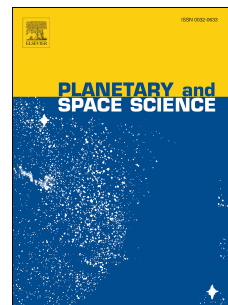
**HAL** is a multi-disciplinary open access archive for the deposit and dissemination of scientific research documents, whether they are published or not. The documents may come from teaching and research institutions in France or abroad, or from public or private research centers.

L'archive ouverte pluridisciplinaire **HAL**, est destinée au dépôt et à la diffusion de documents scientifiques de niveau recherche, publiés ou non, émanant des établissements d'enseignement et de recherche français ou étrangers, des laboratoires publics ou privés.

# Accepted Manuscript

Identification of organic molecules with a laboratory prototype based on the Laser Ablation-CosmOrbitrap

L. Selliez, C. Briois, N. Carrasco, L. Thirkell, R. Thissen, M. Ito, F.-R. Orthous-Daunay, G. Chalumeau, F. Colin, H. Cottin, C. Engrand, L. Flandinet, N. Fray, B. Gaubicher, N. Grand, J.-P. Lebreton, A. Makarov, S. Ruocco, C. Szopa, V. Vuitton, P. Zapf



PII: S0032-0633(18)30266-6

DOI: <https://doi.org/10.1016/j.pss.2019.03.003>

Reference: PSS 4651

To appear in: *Planetary and Space Science*

Received Date: 25 July 2018

Revised Date: 7 March 2019

Accepted Date: 11 March 2019

Please cite this article as: Selliez, L., Briois, C., Carrasco, N., Thirkell, L., Thissen, R., Ito, M., Orthous-Daunay, F.-R., Chalumeau, G., Colin, F., Cottin, H., Engrand, C., Flandinet, L., Fray, N., Gaubicher, B., Grand, N., Lebreton, J.-P., Makarov, A., Ruocco, S., Szopa, C., Vuitton, V., Zapf, P., Identification of organic molecules with a laboratory prototype based on the Laser Ablation-CosmOrbitrap, *Planetary and Space Science* (2019), doi: <https://doi.org/10.1016/j.pss.2019.03.003>.

This is a PDF file of an unedited manuscript that has been accepted for publication. As a service to our customers we are providing this early version of the manuscript. The manuscript will undergo copyediting, typesetting, and review of the resulting proof before it is published in its final form. Please note that during the production process errors may be discovered which could affect the content, and all legal disclaimers that apply to the journal pertain.

1 Identification of organic molecules with a laboratory prototype based  
2 on the Laser Ablation-CosmOrbitrap

3 L. Selliez<sup>1,2, (corresponding author)</sup>, C. Briois<sup>1</sup>, N. Carrasco<sup>2,8</sup>, L. Thirkell<sup>1</sup>, R. Thissen<sup>3</sup>, M. Ito<sup>4</sup>, F.-R.  
4 Orthous-Daunay<sup>5</sup>, G. Chalumeau<sup>1</sup>, F. Colin<sup>1</sup>, H. Cottin<sup>6</sup>, C. Engrand<sup>7</sup>, L. Flandinet<sup>5</sup>, N. Fray<sup>6</sup>, B.  
5 Gaubicher<sup>1</sup>, N. Grand<sup>6</sup>, J.-P. Lebreton<sup>1</sup>, A. Makarov<sup>9</sup>, S. Ruocco<sup>2</sup>, C. Szopa<sup>2,8</sup>, V. Vuitton<sup>5</sup>, P.  
6 Zapf<sup>6</sup>

7 1-LPC2E, UMR CNRS 7328, Université d'Orléans, Cedex 2, France

8 2-LATMOS/IPSL, UVSQ Université Paris Saclay, UPMC Univ. Paris 06, Guyancourt, France

9 3-Laboratoire de Chimie Physique, CNRS, Univ. Paris Sud, Université Paris-Saclay, 91405,  
10 Orsay, France

11 4-Kochi Institute for Core Sample Research, Japan Agency for Marine-Earth Science and  
12 Technology, Kochi, Japan

13 5-Univ. Grenoble Alpes, CNRS, CNES, IPAG, 38000 Grenoble, France

14 6-LISA, UMR CNRS 7583, Université Paris Est Créteil et Université Paris Diderot, Institut  
15 Pierre Simon Laplace, France

16 7-CSNSM, CNRS/IN2P3, Univ. Paris Sud, Université Paris Saclay, Orsay France

17 8- Institut Universitaire de France (IUF), Paris, France

18 9- Thermo Fisher Scientific (Bremen) GmbH, Germany

19 Corresponding author:

20 Laura Selliez

21 Laboratoire de Physique et Chimie de l'Environnement et de l'Espace (LPC2E), UMR CNRS 7328,

22 3A, avenue de la Recherche Scientifique

23 45071 Orléans cedex 2, France

24 e-mail : laura.selliez@cnrs-orleans.fr

25

26 Keywords:

27 Astrobiology; Space mass spectrometry; High mass resolution; Chemical identification; Orbitrap;

28 CosmOrbitrap

29

30

ACCEPTED MANUSCRIPT

## Abstract

31  
32 In the Solar System, extra-terrestrial organic molecules have been found on cometary primitive  
33 objects, on Titan and Enceladus icy moons and on Mars. Identification could be achieved for simple  
34 organic species by remote sensing based on spectroscopic methods. However *in situ* mass  
35 spectrometry is a key technology to determine the nature of more complex organic matter. A large  
36 panel of mass spectrometers has already been developed for space exploration combining different  
37 types of analysers and ion sources. Up to now the highest mass resolution reached with a space  
38 instrument is 9,000 at  $m/z$  28 and corresponds to the DFMS-ROSINA instrument (Balsiger et al., 2007)  
39 dedicated to the study of the comet 67P/Churyumov-Gerasimenko's atmosphere and ionosphere, in  
40 a low pressure environment. A new concept of mass analyser offering ultra-high mass resolving  
41 power of more than 50,000 at  $m/z$  56 (under high vacuum condition about  $10^{-9}$  mbar) is currently  
42 being developed for space applications: the CosmOrbitrap (Briois et al., 2016), based on the  
43 Orbitrap™ technology.

44 This work challenges the use of LAb-CosmOrbitrap, a space instrument prototype combining Laser  
45 Ablation ionisation and the CosmOrbitrap mass analyser, to identify solid organic molecules of  
46 relevance to the future space exploration. For this purpose a blind test was jointly organised by the  
47 JAXA-HRMS team (Japan Aerospace Exploration Agency-High Resolution Mass Spectrometry) and the  
48 CosmOrbitrap consortium. The JAXA team provided two organic samples, whereas the CosmOrbitrap  
49 consortium analysed them without prior information. Thanks to the high analytical performances of  
50 the prototype and our HRMS data post-processing, we successfully identified the two molecules as  
51 HOBt, hydroxybenzotriazole ( $C_6H_5N_3O$ ) and BBOT, 2,5-Bis(5-tert-butyl-benzoxazol-2-yl)thiophene  
52 ( $C_{26}H_{26}N_2O_2S$ ), with a mass resolving power of, respectively, 123 540 and 69 219. The success of this  
53 blind test on complex organic molecules shows the strong potential of LAb-CosmOrbitrap for future  
54 space applications.

55

56

57 *Highlights:*

- 58 • Efficient ionisation of solid sample by nano-pulsed single laser shot
- 59 • Powerful analytical performances of CosmOrbitrap mass analyser
- 60 • Successful blind test identification of organics ionised by Laser-CosmOrbitrap
- 61 • Laser-CosmOrbitrap relevant technique for space exploration of organic rich worlds

## 62 I) Introduction

63

64 The capability to study organic molecules and organic-rich environments in the Solar System is  
65 important for astrobiology (Horneck, 1995). This allows a better understanding of the chemical  
66 evolution that leads to the emergence of Life on Earth and provides constraints on the possible  
67 habitability of other planets or moons. Detection of organic molecules and traces of extinct or extant  
68 Life is therefore driving space exploration concepts for objects like Europa, Titan and Enceladus.  
69 Many space missions to these objects are either in preparation or proposed: the JUICE (JUperiter ICy  
70 moons Explorer) mission (Grasset et al., 2013), the Europa Clipper mission (Phillips and Pappalardo,  
71 2014) or, among others, the Dragonfly mission (Principal Investigator E. Turtle, see the JHU/APL  
72 website for further details) selected in 2017 as finalist of the NASA New Frontiers program.

73 One of the best analytical tools used in space missions for chemical analysis is mass spectrometry.  
74 This technique allows to assess the molecular composition of the environments studied. The  
75 detection and the identification of compounds lead to a better understanding of the chemistry  
76 occurring on diverse objects of the Solar System. A high diversity in terms of targets studied (planets,  
77 moons, small bodies etc.) and sample types (solid rocks, gaseous compounds in atmosphere,  
78 aerosols, ions etc.) is possible. In part, this is due to the multiple combinations of ion sources and  
79 mass analysers existing. Mass spectrometers have been boarded since the beginning of the space  
80 exploration and are still an instrument family essential to the future space missions. On the Cassini-  
81 Huygens mission, the instruments INMS (Ion and Neutral Mass Spectrometer) (Waite et al., 2004) or  
82 CAPS (CAssini Plasma Spectrometer) (Young et al., 2004) enabled the collection of a large amount of  
83 data and the improvement of our knowledge about Titan upper atmosphere (Waite et al., 2007) and  
84 Enceladus plumes (Waite et al., 2017). Thanks to modelling, attributions of a number of peaks in  
85 INMS data were successfully proposed, up to  $m/z < 100$ . However, the mass resolution of these  
86 instruments (including INMS) did not enable to directly decipher the composition of the complex  
87 organic matter. That explains why the moons of Saturn are still highly requested in the discovery

88 programs of space agencies. The best mass resolving power ( $m/\Delta m$  or MRP at Full-Width Half  
89 Maximum (FWHM)) of a space mass spectrometer, was provided by the DFMS (Double Focusing  
90 Magnetic Mass Spectrometer) instrument of the ROSINA (Rosetta Orbiter Spectrometer for Ion and  
91 Neutral Analysis) experiment on board the Rosetta mission with  $m/\Delta m$  9,000 FWHM at  $m/z$  28  
92 (Balsiger et al., 2007). With these performances, the detection of species like  $N_2$  and  $O_2$  on a comet  
93 was made possible for the first time (Bieler et al., 2015; Rubin et al., 2015). In addition, a prebiotic  
94 compound, the amino acid glycine, at  $m/z$  75, has been detected (Altwegg et al., 2016). Despite its  
95 high MRP, ROSINA/DFMS covered a mass range from 12 to 150 mass units (u) excluding the analysis  
96 of heavy organic molecules about hundreds of mass units.

97 It became a critical need to develop a new generation of mass spectrometers to go further in these  
98 studies, with high analytical performances required. In term of mass accuracy, a range of less than 1  
99 to 5 ppm is needed in order to provide relevant molecular formula attributions. About the MRP, few  
100 tens of thousands (from 50,000 to 100,000) allow the separation of isobaric interferences at high  $m/z$   
101 (up to  $m/z$  500) of organic species with, for instance, an exobiological interest. Detection and  
102 identification of complex organic molecules involved in chemical mechanisms occurring on Solar  
103 System bodies, such as the organic chemistry observed on Titan (Hörst, 2017) are thus possible. In  
104 the laboratory, the Orbitrap<sup>TM</sup> technology is now currently applied to the analysis of complex organic  
105 material of interest to space exploration, such as analogues of Titan's aerosols (Pernot et al., 2010)  
106 and soluble organic matter of meteorites (Bonnet et al., 2013; Gautier et al., 2016; Orthous-Daunay  
107 et al., 2013). It enables to cover a dynamic mass range, up to several thousands in mass units  
108 (Makarov, 2000), with a data acquisition time of about 1 second.

109 A mass analyser designed for space and based on the Orbitrap technology is currently being  
110 developed under the name of CosmOrbitrap (Briois et al., 2016), which would bring a technical  
111 breakthrough for direct *in situ* analysis. Mainly based on the analysis of metals with a LAb-  
112 CosmOrbitrap prototype, Briois et al., 2016 have shown the high analytical performances of this mass  
113 spectrometry technique, expecting this mass analyser to be part of a future space mass



114 spectrometer. In this previous work, high performances have been achieved with a simple  
115 instrumental configuration of the prototype using direct laser ablation ionisation coupled with a  
116 CosmOrbitrap mass analyser through an Einzel lens. They obtained mass resolutions at FWHM of  
117 474,000 on beryllium ( $m/z$  9) and of 90,000 on lead ( $m/z$  208), close to mass resolution of 60,000 at  
118  $m/z$  400 obtained with a commercial LTQ-Orbitrap XL instrument (Perry et al, 2008). Briois et al, 2016  
119 have demonstrated a mass accuracy within less than 15 ppm over the 12 to 115  $m/z$  range with the  
120 LAb-CosmOrbitrap prototype, rather larger than the 1-5 ppm given by commercial Orbitrap™ based  
121 instruments.

122 The present work focuses on the capability of the LAb-CosmOrbitrap to provide molecular  
123 identification, another important question in the development of a space instrument, by performing  
124 a blind test on two different molecules. Under a Japanese/French collaboration framework, two  
125 organic samples have been chosen by the JAXA HRMS team and sent to the CosmOrbitrap team  
126 without any information on their chemical composition. This work reports the blind analysis  
127 performed on these two “unknown” samples by the CosmOrbitrap consortium with the LAb-  
128 CosmOrbitrap prototype in order to identify them. Updates on the analytical performances of the  
129 LAb-CosmOrbitrap, on organics, are also given.

130

131

## 132 II) Methods

133

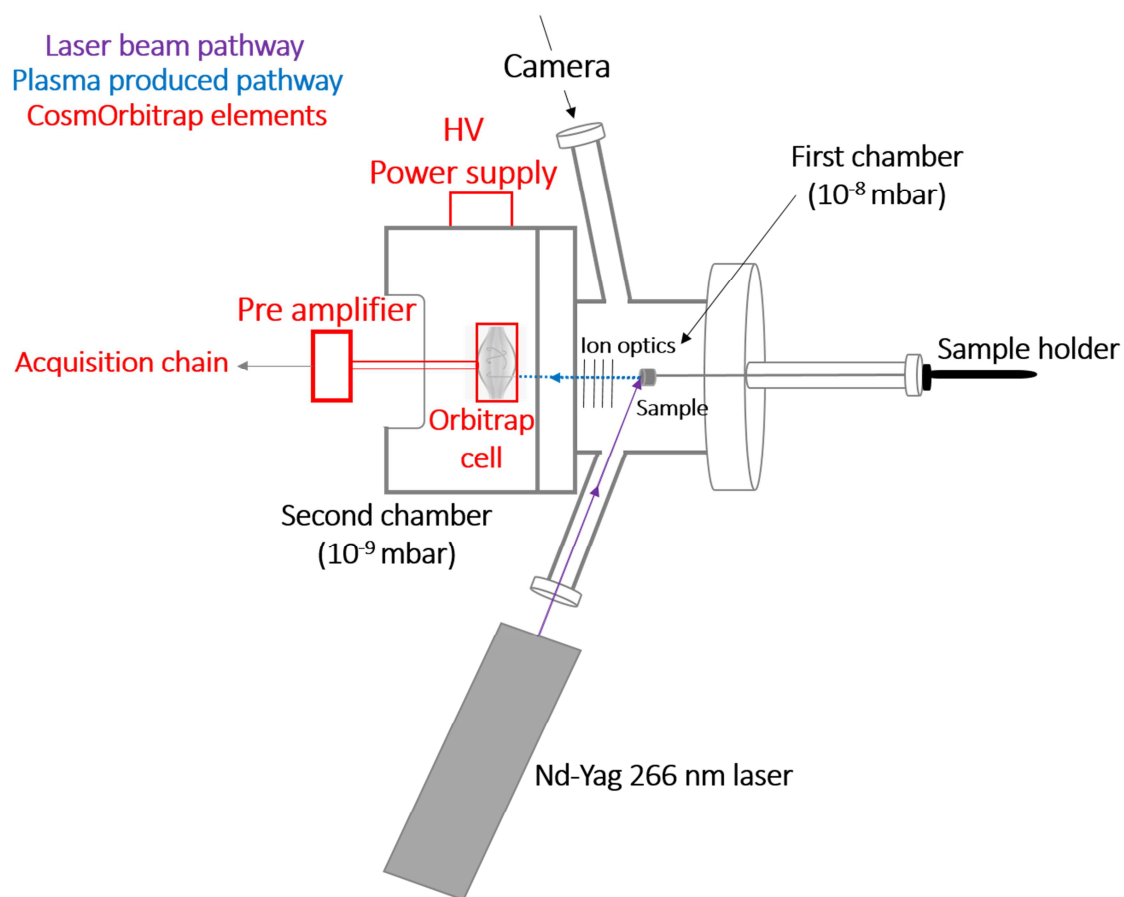
## 134 a) The laser ablation – CosmOrbitrap prototype

135 The blind test experiments have been conducted using a slightly modified version of the laboratory  
136 prototype previously described in Briois et al., 2016. To provide a better absorption of organic  
137 molecules in the UV resulting into a more efficient ionisation, the UV nitrogen laser at 337 nm was  
138 exchanged for a Nd-YAG laser at 266 nm (Goesmann et al., 2017). The latter is the “Brilliant” model  
139 provided by Quantel, with 4 ns pulse duration and about 100  $\mu\text{J}$  energy per pulse. The angle of  
140 incidence on the surface of the sample-holder is  $50^\circ$ , resulting in an elliptical shape of the footprint of  
141 the laser beam with a minor axis of typically 30  $\mu\text{m}$  and a major axis of 40  $\mu\text{m}$  (measured on silicon  
142 wafer) and energy density of  $15 \text{ J}\cdot\text{cm}^{-2}$ .

143 The Orbitrap mass analyser cell commercialised by the Thermo Fisher Scientific (Bremen, Germany) is  
144 an ion trap in which ions are oscillating in a confining quadro-logarithmic electric field produced by  
145 barrel-shaped electrodes. The geometry of the cell and the injection of ions by electrodynamic  
146 squeezing was developed by A. Makarov (Makarov, 2000). The Orbitrap cell consists of two external  
147 electrodes, one central electrode and a deflector electrode. External electrodes are kept at the  
148 ground potential. Ions are injected in the cell after 1.1 kV acceleration, while a transition of the high  
149 voltage (from nominal voltages -2500 V to -3500 V) is applied to the central electrode and (from 0 to  
150 350 V) to the deflector electrode. All experiments have been carried out in positive ion mode. We  
151 note that negative ions can also be studied by reverting the high voltages on the source, the central  
152 and the deflector electrodes. Due to the quadratic potential in the longitudinal direction, trapped  
153 ions oscillate at a frequency proportional to their mass to charge ( $m/z$ ) ratio. The pulsation  $\omega$  (in  
154 rad/s) and the  $m/z$  ratio are linked by the formula:  $\omega = (k*(z/m))^{1/2}$ , where  $k$  is a parameter depending  
155 on the shape and the voltage applied on electrodes (Makarov et al., 2009; Perry et al., 2008). This

156 oscillation creates a perturbation of the potential difference between the external electrodes,  
157 providing the signal analysed by the instrument electronics.

158 Figure 1 represents the laboratory test bench used in this study. The Nd-YAG laser at 266 nm is used  
159 for ablation and ionisation. The prototype is composed of two vacuum chambers. The first one  
160 contains the sample at  $10^{-8}$  mbar. Solid samples can be analysed, as they are usually pressed or  
161 dropped on the metallic surface of a small sample-holder (8 mm height, 7 mm diameter) itself  
162 screwed at the extremity of a rod. The second vacuum chamber contains the Orbitrap cell and is  
163 maintained at a pressure of  $10^{-9}$  mbar. Both vacuum chamber are linked by a differential pumping  
164 system. The aperture between both vacuum chambers is smaller than 2 mm. Two antennas, one on  
165 each external electrodes of the Orbitrap cell, are directed to the pre-amplifier. The whole  
166 configuration is named LAb-CosmOrbitrap, standing for Laser Ablation CosmOrbitrap. As defined in  
167 Briois et al., 2016, the CosmOrbitrap **space** mass analyser includes the following elements (in red in  
168 Figure 1): the Orbitrap cell itself and its retaining ring, the ultra-stable high voltage power supply, the  
169 pre-amplifier and the data acquisition / command control board cards. These elements, composing  
170 the CosmOrbitrap, are involved in a TRL (Technology Readiness Level) development. TRL is a scale  
171 used by space agencies, such as NASA, with 9 levels. The first one (TRL 1) is the basic principle, an  
172 idea of a concept and the last one (TRL 9) a real system, on-board and operational. CosmOrbitrap  
173 elements are at an intermediate level, TRL 3, indicating they are laboratory elements set up as a  
174 proof-of-concept.



175

176 *Figure 1: LAb-CosmOrbitrap laboratory prototype at LPC2E (Orléans). The Nd-YAG laser is used as ablation/ionisation*  
 177 *process. The first vacuum chamber holds the sample for ablation and ions extraction. The second chamber contains the*  
 178 *Orbitrap cell for the mass analysis. Both chambers are connected by a 2 mm feedthrough. In red are reported the*  
 179 *CosmOrbitrap elements involved in a TRL development for space applications. In the present work, CosmOrbitrap elements*  
 180 *are at TRL 3.*

181

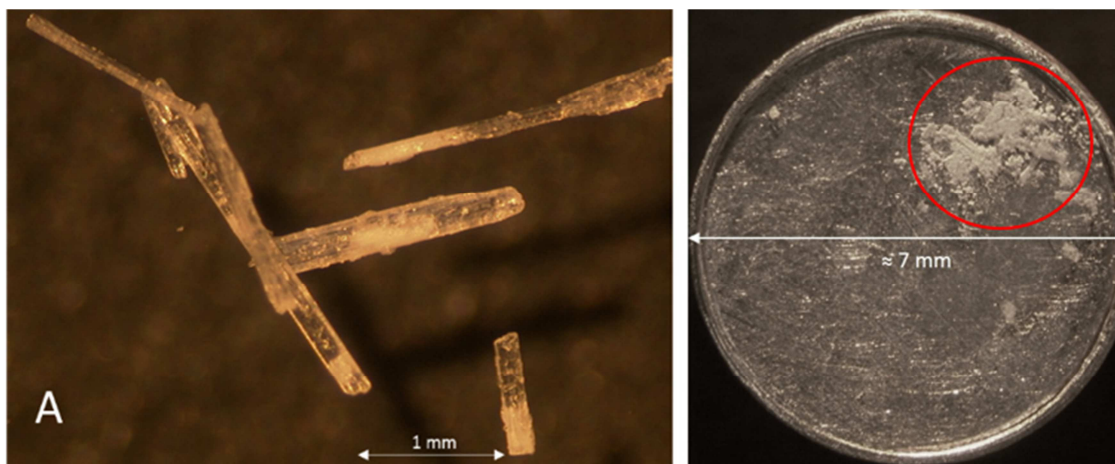
182 The acquisition software (Alyxan) allows visualising in real time both the frequency transient signal  
 183 and the mass spectrum transient signal processed by Fast Fourier Transform (FFT). The signal is  
 184 recorded during 838 ms with a sampling frequency of 5 MHz inducing the storage of 4 192 304  
 185 points, for a single packet of ions. A Hann window is applied before the FFT treatment.

186

## 187 b) Sample preparation

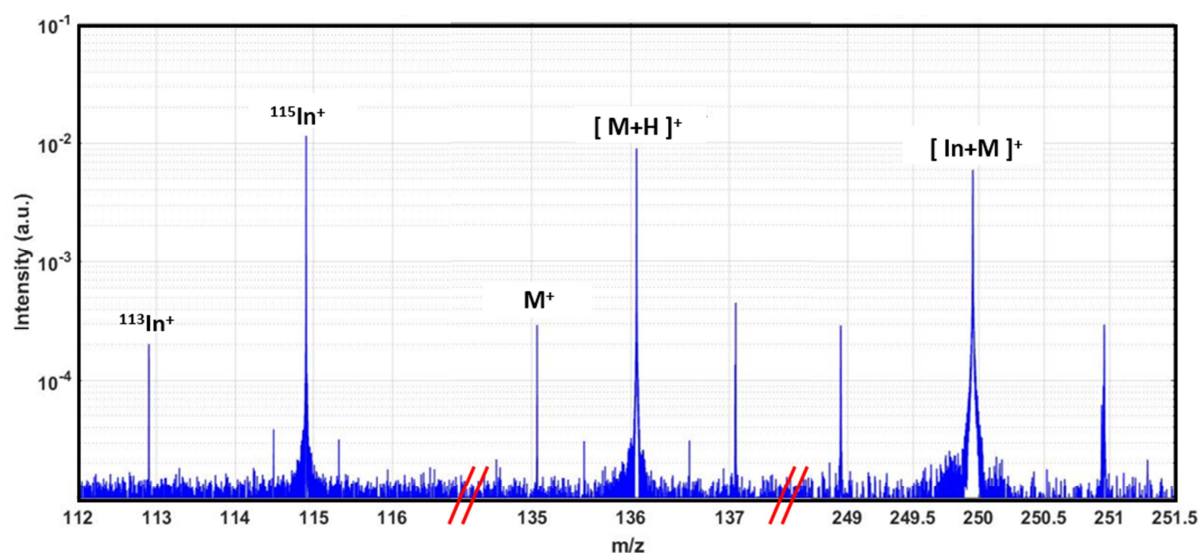
188 Few milligrams of two samples, named A and B, have been supplied by JAXA HRMS team to  
 189 CosmOrbitrap team. The samples are respectively white and green sticks (see Figure 2 for sample A).

190 A few sticks of each sample are collected and put on a different indium sample-holder. Sticks are  
191 pressed using an agate pestle to be embedded onto the indium target (Goodfellow, high purity:  
192 99,999%, rolled) previously cleaned under consecutive ultrasonic baths of acetone and n-Hexane.  
193 The indium targets and the sample deposit are fed into the first vacuum chamber (Figure 1).



194  
195 *Figure 2: Pictures obtained with an optical microscope of Sample "A" as it was received from the JAXA HRMS team (left) and*  
196 *pressed on the sample holder (right, in the red circle).*

197  
198 This simple sample preparation provides a useful internal reference for mass calibration with the  
199 positive ion of indium major isotope peak at  $m/z$  114.903, and possible cluster ions between the  
200 sample (M) and the indium ion as  $[\text{In}+\text{M}]^+$ ,  $[\text{In}+2\text{M}]^+$ ,  $[2\text{In}+\text{M}]^+$ , which help for the identification of the  
201 parent mass M. These clusters are also observed with other mass spectrometry techniques  
202 (Bhardwaj and Hanley, 2014; Carrasco et al., 2016; Le Roy et al., 2015) and with the LAb-  
203 CosmOrbitrap on another organic molecule, adenine ( $\text{C}_5\text{H}_5\text{N}_5$ ) observed at  $m/z$  135.0545  
204 (unpublished data from the study of Briois et al., 2016). Adenine is studied in pure solid form (thin  
205 white powder) and Figure 3 shows a detail of a mass spectrum obtained from the analysis of adenine  
206 powder pressed onto an indium surface (as it was done for samples A and B studied in this work).  
207 Both indium isotopes ( $^{113}\text{In}^+$  and  $^{115}\text{In}^+$ ) are visible, as well as the adenine protonated peak  $[\text{M}+\text{H}]^+$ .  
208 Cluster of the molecular ion of adenine associated with indium  $[\text{In}+\text{M}]^+$  is observed at the nominal  
209  $m/z$  250.



210

211 *Figure 3: Detail of a mass spectrum of adenine (M) powder pressed on an indium surface showing the formation of clusters*  
 212 *between the sample-holder (indium) and adenine. The left mass window shows the indium main isotope peak  $^{115}\text{In}^+$  and its*  
 213 *isotope at  $m/z$  113. The mass window in the middle details the molecular ion peak of adenine ( $M^+$ ) and its protonated ion*  
 214  *$[\text{M}+\text{H}]^+$ . One mass unit higher, at  $m/z$  137, we observe an isotopologue of the adenine protonated ion. The right mass*  
 215 *window shows the cluster formed between the indium ion  $^{115}\text{In}^+$  and the neutral adenine M. This  $[\text{In}+\text{M}]^+$  peak is surrounded*  
 216 *by two other peaks at nominal  $m/z$  249 and 251, meaning at one hydrogen mass lower and higher. Peaks at  $m/z$  114.5,*  
 217 *115.3, 135.5, and 136.6 are artifacts due to the FFT treatment*

218

219 The presence of the indium peak is also an indicator of the laser beam position, as it disappears from  
 220 the spectrum when the laser beam irradiates the selected organic samples which absorb less energy  
 221 from the 266 nm UV laser in this setup. At the edge of the sample and the sample-holder, both are  
 222 visible on the spectrum (Figure 3).

223

### 224 c) Validation of the ionisation method for the blind test

225 Tests are performed on the sample with a progressive increase of the laser power from 30  $\mu\text{J}$  up to  
 226 750  $\mu\text{J}$ , until a complex specific pattern is observed in the spectrum. A systematic study of the mass  
 227 spectra as a function of the laser power was not possible, due to the too small amount of sample  
 228 available. One of the main features of laser ablation ionisation (LAb) with organic molecules is the  
 229 fragmentation resulting from the dissociative ionisation of the sample. This can induce a high

230 variability and diversity of mechanisms generating the mass spectrometric signature for organic  
231 molecules, which is not observed for metal, essentially resulting in singly charged atomic ions and  
232 clusters. Clusters are positively charged entities from the addition of one metallic ion coming from  
233 the surface of the sample-holder to a neutral organic molecule thermo-desorbed from the sample, as  
234 described in the previous section.

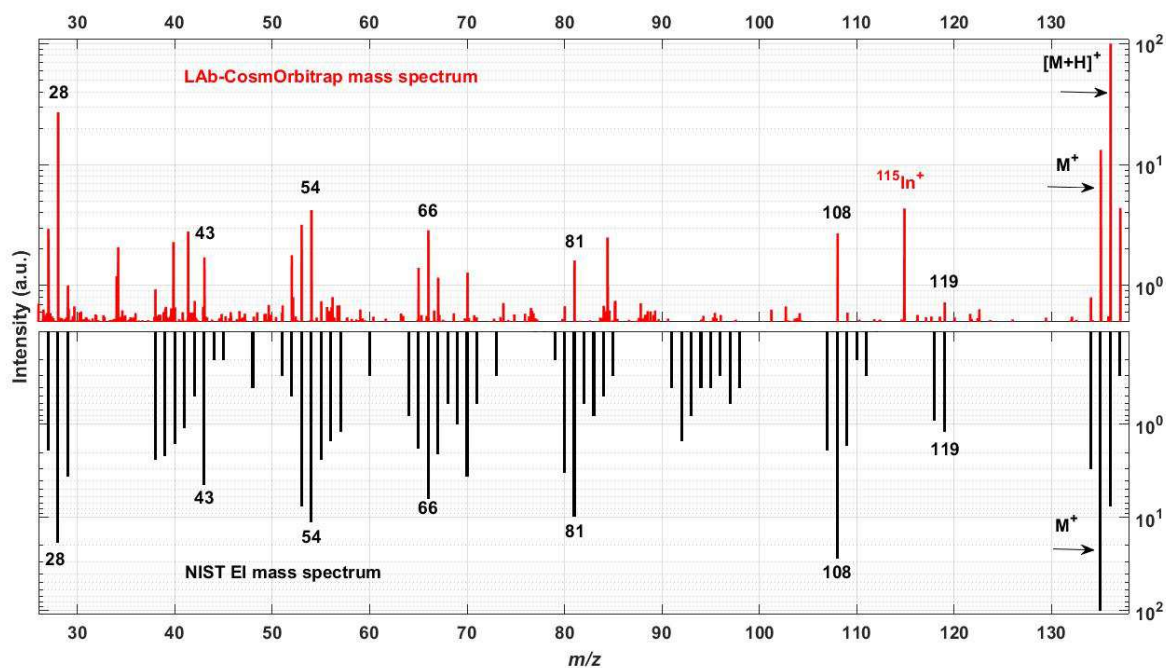
235 To ensure that this ionisation method is relevant for this blind test study and appropriate in the  
236 context of a space configuration, we compare the mass spectrometric signature of adenine obtained  
237 on the one hand by the well-documented electron ionisation process at 70 eV (NIST database) and  
238 on the other hand by the LAb technique of our prototype (Figure 4). Similarities in the fragmentation  
239 patterns are observed between both mass spectra. The top panel, in red, shows a LAb-CosmOrbitrap  
240 mass spectrum. The lower panel, in black and with a reverse y-scale, shows the electron ionisation  
241 mass spectrum, recovered from the NIST database. Intense peaks and parent molecules are  
242 identified on the mass spectra. Intensities of ions detected are different but main fragment ions are  
243 the same for both ionisation processes. Two of the most intense fragment ions are at  $m/z$  28 and  
244 108. The fragment ion at  $m/z$  108 is interpreted as a loss of an HCN molecule from the adenine  
245 molecular ion observed at  $m/z$  135.0527. Based on exact masses calculations, the  $m/z$  108 fragment  
246 ion is expected at  $m/z$  108.0431. We observed it at  $m/z$  108.0427 (-3.7 ppm). Laser ablation and  
247 electron ionisation (EI) are no soft ionisation processes and produce molecular ions and subsequent  
248 fragmentations. The fragmentation results from molecular ions presenting an unstable structure due  
249 to (1) the loss of an electron from the electronic cloud and (2) the internal energy left in the ionic  
250 species, imparted either by the incident electron or the plasma generated by the laser. For a given  
251 molecular structure, the fragmentation routes that results from this process should be similar. This  
252 explains why the main fragment ions observed are similar with both ionisation methods. However  
253 differences of peak intensities are observed between the two mass spectra. This is the signature that  
254 the internal energy imparted in the ablation plasma is different from the one imparted by the 70 eV  
255 electrons. This is understandable as the laser generates micron size plasma, with a lifetime of

256 hundreds of nanoseconds. This is a medium presenting, from the ion microphysical point of view,  
257 very diverse conditions. Hence, the ion can be generated in the middle of the plasma plume or close  
258 to its edges, or it can be generated at the beginning of the ablation process, in high density of  
259 charges and gaseous species, or later on, during the recombination steps following the photon  
260 extinction. This variability in time and position results in different amount of internal energy  
261 imparted to the primary ions, leading to different probability to further evolve into fragments. A  
262 further difference is in the repeatability of the spectra. Hence with electron ionisation, the energy  
263 used is constant, whereas the shot to shot laser variability is about 10%. Moreover, as we press solid  
264 powders onto indium, the surface of the sample is not homogenous and varies from one laser shot to  
265 another. This induces inherent variabilities among the LAb-CosmOrbitrap mass spectra.

266 The main difference in the LAb-CosmOrbitrap spectrum, compared to the NIST spectrum, is an  
267 important contribution at  $m/z$  136. The MRP (FWHM) of 123,080 enables to identify the protonated  
268 ion of adenine  $[M+H]^+$  at  $m/z$  136.0614. It excludes the signature of  $^{13}\text{C}$  and  $^{15}\text{N}$  natural  
269 isotopologues of adenine at  $m/z$  136.0574 and 136.0510, respectively, which would have been  
270 detected in the mass spectrum, in view of the mass resolution. The presence of this protonated ion  
271 results from proton addition by ion molecule reactions occurring inside the plume.

272





273  
 274 *Figure 4: Mass spectra of adenine obtained with Lab-CosmOrbitrap (red, upper panel) and from the NIST (black, lower panel,*  
 275 *inverted scale) showing a comparison of the fragmentation patterns of adenine ( $M$ ) between both ionisation processes:*  
 276 *laser ablation and electron impact. On CosmOrbitrap spectrum, we see the molecular ion of adenine ( $M^+$ ) and the*  
 277 *protonated ion ( $[M+H]^+$ ) both in positive mode. On the NIST spectrum, we observe only the molecular ion.*

278  
 279 The clear similarities observed between the two spectra of adenine allow us to conclude that  
 280 adenine can be identified with the fragmentation patterns obtained in our experiment by  
 281 comparison with its electron impact fingerprint provided in the NIST database. Note that obvious  
 282 discrepancies are also observed, for instance in the  $m/z$  range 30 to 40 and 90 to 100. In our case, the  
 283 applied laser power is only high enough to induce a fragmentation pattern. With a higher laser  
 284 power, more fragment ions would be formed and detected. The electron impact ionization used to  
 285 obtain mass spectra referenced in the NIST database involves a similar dissociating ionization  
 286 process, breaking the molecular ion. For one given molecule, some fragments are produced with a  
 287 higher probability which highly depends on the spatial configuration of the molecule and its chemical  
 288 bonds. Electron impact ionization and laser ablation are preferentially producing the same fragments  
 289 and it is why we observe the main fragment ions at the closest masses from the molecular ion in the  
 290 mass spectra. However, the NIST mass spectrum shows more fragmentation peaks at lower masses

291 than in our mass spectrum. This suggests that the electron ionization at 70 eV is more energetic than  
292 the photo-ionisation process induced by the 266 nm laser used (corresponding to 4.6 eV for one-  
293 photon transitions). The goal of this comparison (and of those which will be presented in the results  
294 section) is to confirm the attribution of a molecular formula and the identification of a compound by  
295 finding similar fragment ions between both techniques. We are not looking for two identical mass  
296 spectra but only a few and consistent similarities between both in order to confirm our identification.  
297 The fragmentation becomes a key asset and the final step in the identification process of a molecule  
298 and consequently the choice of the laser ablation as ionisation system has been found relevant for  
299 the blind test study.

300

#### 301 d) Data processing procedures for the blind test

302 Data processing of the spectra is made with the in-house Attributor software of HRMS analysis  
303 (described at <https://frodsite.wordpress.com/research/attributor/>) developed in the Igor Pro  
304 environment. A Hann apodisation window and 3 zero padding (signal of 4 million points associated to  
305 12 million points set to 0) are applied before a [6-838] ms FFT. Mass calibration is performed on the  
306  $^{115}\text{In}^+$  peak.

307 The study is based on two data representations: (1) the formal mass spectrum and (2) the “Mass  
308 Defect versus Exact Mass” diagram (MDvEM diagram). The latter represents the mass defect of each  
309 ion as a function of its exact mass. The mass defect (MD) of an element is the mass difference  
310 between its exact mass and its closest integer mass (Murray Kermit K. et al., 2013). By convention,  
311 the mass defect of Carbon ( $\text{MD}_{\text{Carbon}}$ ) is set to 0. Indeed, its exact mass is 12 u, which already is the  
312 integer mass. If we consider the nitrogen element: its exact mass is 14.0031 u and the closest integer  
313 mass is 14 u. The difference between both gives a positive mass defect of +0.0031 u. On the contrary,  
314 indium shows a negative mass defect: the exact mass is 114.9038 u and the closest integer mass 115  
315 u, yielding a negative mass defect of -0.0962 u. A valuable asset of this kind of diagram is the  
316 observation of specific trend lines. They are representative of repetitive molecular groups thus they

317 act as molecular signatures. They allow us to make assumptions on the possible molecular groups  
318 and/or elements composing the molecule (as described in the results section and shown in Figure 6  
319 & Figure 9). Artifact peaks (mostly some vertical alignments of points due to ringing phenomenon)  
320 are easily detected with this analytical representation, which allows to discard them.

321 Our identification steps, based on the study of the two data representations enounced and described  
322 above, are: (1) to find the parent peak, this means the  $m/z$  of the peak to identify; (2) to determine  
323 the molecular formula: for this, we make some assumptions on elements possibly composing the  
324 molecule and their occurrence (hydrogen and carbon are directly supposed to be present as we are  
325 looking for organic compounds but nitrogen, sulphur, oxygen or phosphorous can also be part of the  
326 molecular formula); (3) to confirm our identification based on the comparison of mass spectra from  
327 the NIST database (electron ionisation at 70 eV) and LAb-CosmOrbitrap mass spectra. This  
328 comparison is performed, for the selected species, by looking for a match of the same main fragment  
329 ions in both mass spectra (as described in the previous section).

330 The determination of the molecular formula (step 2) is done with the Attributor software which  
331 calculates combinations of molecular formula at one  $m/z$  given. Each combination calculated is given  
332 with its mass accuracy (based on the difference between the theoretical  $m/z$  and the observed one)  
333 in ppm. Within this list of candidates, the most interesting ones (depending on their mass accuracy)  
334 are chosen and then the step 3 starts (comparison of the fragmentation pattern using the NIST  
335 database mass spectra as reference).

336

337

## 338 III) Results

## 339 a) Identification of "sample A"

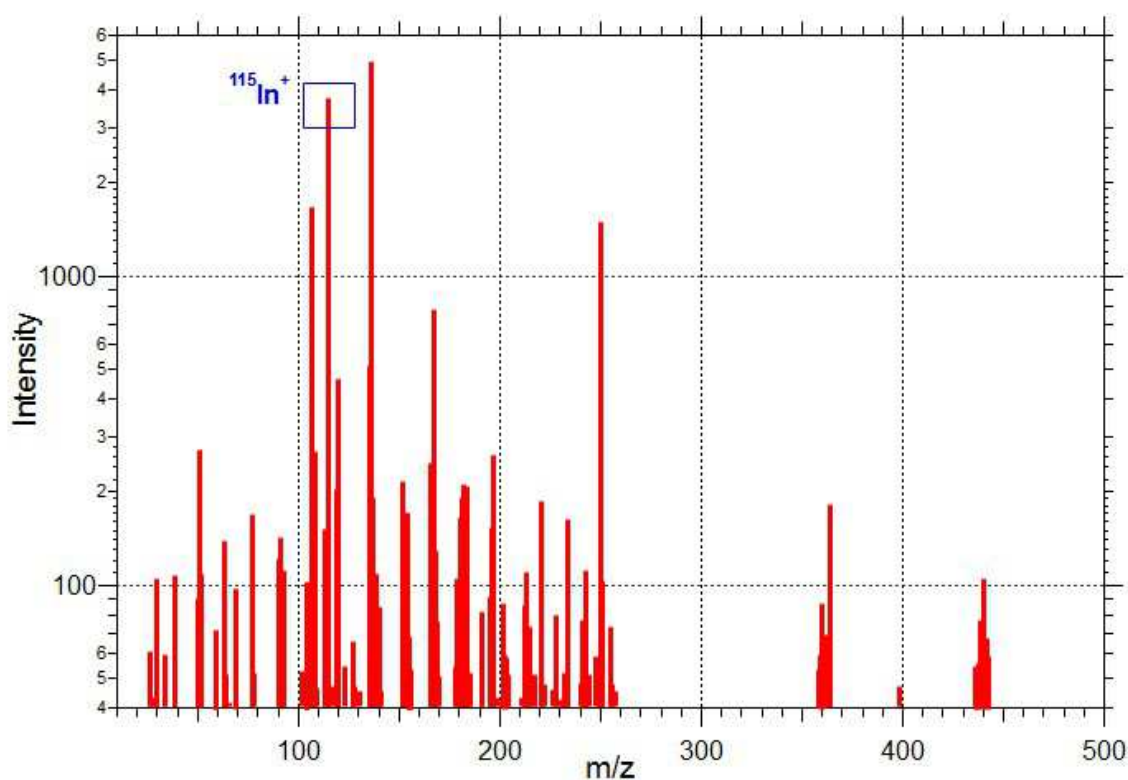
340 The surface of "sample A" is scanned with successive laser shots at different locations on the sample-  
341 holder. A direct visualisation of mass spectra during the data acquisition allows to locate peaks in the  
342  $m/z$  range 50 to 250, with some isolated peaks above  $m/z$  350. Within this quite extended pattern,  
343 the identification of a parent molecule is not obvious. Figure 5 presents a representative mass  
344 spectrum. Among the most intense peaks detected, we observe the main indium isotope coming  
345 from the metallic surface of the sample holder at nominal  $m/z$  115. Among the other intense peaks  
346 detected, nominal  $m/z$  136, 250 and 364 are expected to be organic compound(s) or cluster(s)  
347 between indium and organics. In addition, in view of the large number of peaks detected, we assume  
348 a high fragmentation. This fragmentation is consistent with our laser ablation ionisation process  
349 which, as explained in the method section, induces it. Fragmentation comes from the molecular ion,  
350 then fragments ions produced can be themselves fragmented.

351 Between some clusters of peaks we are thus able to identify losses of only one element such as  
352 carbon, nitrogen, oxygen etc. These losses corresponding to only one element are good indicators for  
353 identifying elements composing the molecular formula. It is what we call "mass spacing": the mass  
354 difference between two peaks. The high MRP of the CosmOrbitrap (up to 90,000 at  $m/z$  208 (lead) as  
355 referenced in the Briois et al., 2016 ) allows to calculate them with a precision of four digits in the  
356  $m/z$  range 50 to 250. The CosmOrbitrap MRP (as for the conventional laboratory Orbitrap) is  
357 decreasing as a function of the square root of  $m/z$  (Briois et al., 2016; Makarov, 2000; Perry et al.,  
358 2008). The power law fitting this evolution of the MRP with the  $m/z$  ratio is given by:  $m/\Delta m = k*(m/z)^{-1/2}$ .  
359 Several nominal mass spacing of 12 u are detected ( $m/z$  11.9999 for instance, attributed to  
360 carbon), but also 14 u ( $m/z$  14.0028, attributed to nitrogen) and 16 u ( $m/z$  15.9946, attributed to  
361 oxygen). Mass spacing of 31.9831 u are observed, which best correspond to losses (or addition) of  
362 two oxygen (mass = 31.9898 u for O<sub>2</sub>). The high precision of this value enables to discard the

363 presence of sulphur in "sample A" ( $m/z$  31.7921). At this time, we are thus looking for a "CHNO"  
364 molecule.

365 The kind of mass spectrum presented on Figure 5 is usually observed at the edge of the sample  
366 deposit or after a series of shots, when the metal target starts to emerge. As mentioned in the  
367 method section, the ionisation of a solid sample deposited on a metal target can produce cluster ions  
368 such as  $[\text{In}+\text{M}]^+$ . Consequently, removing the mass of  $^{115}\text{In}$  to these cluster ions would lead to the  
369 neutral parent mass of sample "A" (molecule M). We obtain a nominal mass of 245 u when  
370 subtracting the mass of one  $^{115}\text{In}$  from the  $m/z$  364 and a nominal mass of 135 u when subtracting  
371 the mass of one  $^{115}\text{In}$  from the  $m/z$  250.

372



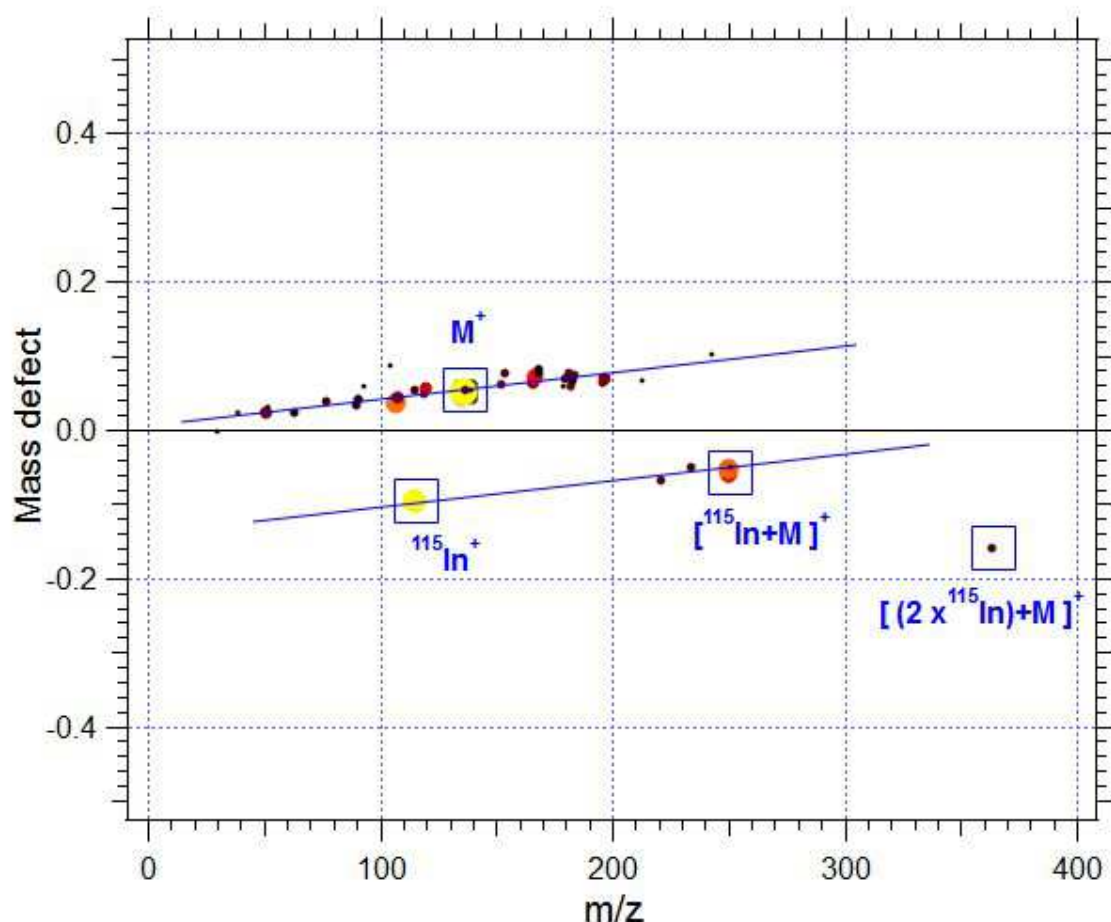
373

374 Figure 5: Overall mass spectrum of sample "A". The blue square indicates the indium peak. Dynamic range is about 25  
375 (based on  $^{115}\text{In}^+$  and  $^{113}\text{In}^+$ ).

376

377

378 Further investigations using MDvEM diagram are performed with Attributor on the formal “sample  
 379 A” mass spectrum as observed in Figure 5, in order to look for cluster ions. The MDvEM diagram is  
 380 presented in Figure 6.



381  
 382 *Figure 6: Mass Defect versus Exact Mass (MDvEM) diagram of the « Sample A ».* Each dot on the diagram corresponds to an  
 383 ion detected in the mass spectrum (Figure 5). The mass defect is represented as a function of the  $m/z$  of each ion. In  
 384 addition, colour and size of the dots are proportional to the logarithm of the intensity of each ion peak. Lighter colours (such  
 385 as yellow then orange) corresponds to the most intense peaks and darker ones (dark red then black) to the less intense  
 386 peaks. Blue lines highlight specific trend lines and cluster ions.

387  
 388 Two different trends are evidenced. The first one (top blue line on Figure 6), with a positive MD, is  
 389 attributed to organic species. Indeed, hydrogen and nitrogen elements have a positive MD  
 390 (respectively +0.0078 and +0.0031), as explained in the method section carbon has a MD equal to 0  
 391 by convention and within these organic elements only the oxygen has a negative MD (-0.0051).

392 Previously, we present mass spacing calculated between peaks on the  $m/z$  range 20 to 250 pointing  
393 toward the presence of a "CHNO" molecule with mainly C, H and N elements. We therefore expect a  
394 parent compound with a positive mass defect.

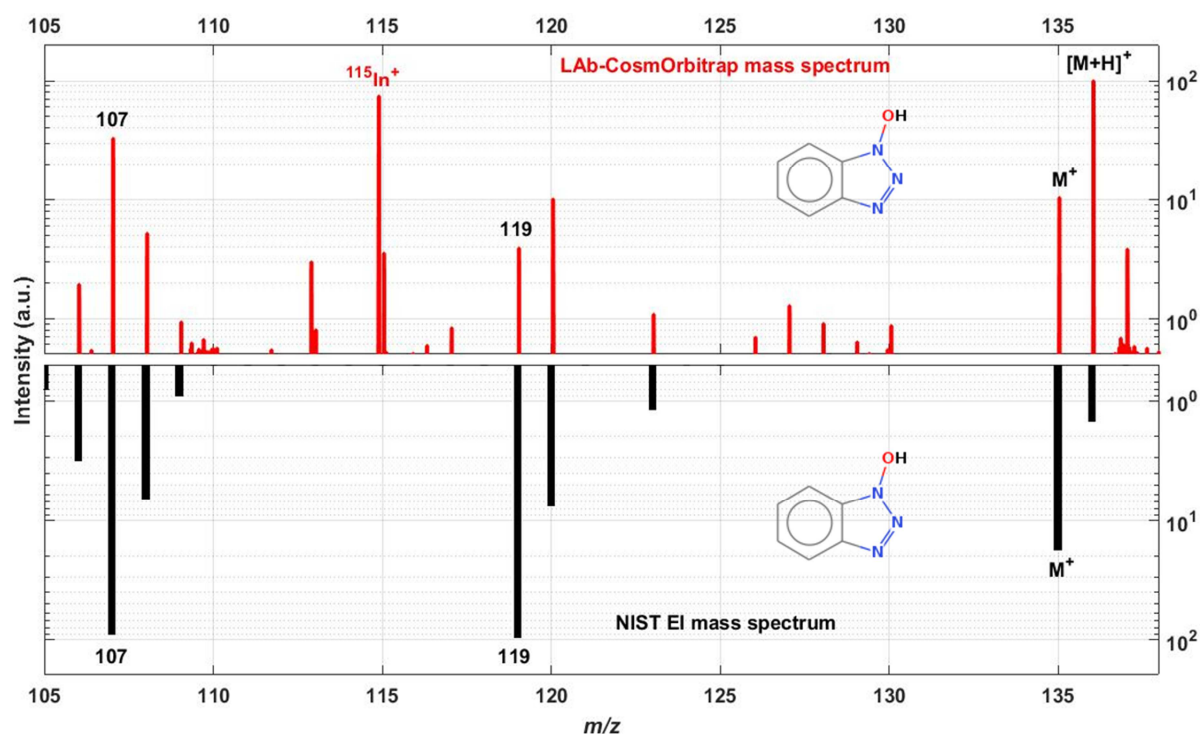
395 The second trend (bottom blue line with negative MD) is linked to the presence of indium, which has  
396 a MD of -0.0962. The yellow point corresponds to the large MD of indium alone, then the other  
397 points on this line corresponds to heteroatoms at higher masses: cluster ions of indium and the  
398 organic compound are suspected at  $m/z$  249.9455 ( $[In+M]^+$ ) and at the nominal  $m/z$  365  $[2In+M]^+$ .

399 From these cluster ions and as calculated previously in this section, we derive a hypothetical  $m/z$  of  
400 the parent peak at 135.0417, consistent with the observed mass of a peak, located at  $m/z$  135.0426.

401 With this laser ablation ionisation process and as demonstrated on adenine in the previous section  
402 we are observing both molecular and protonated ions. Thus, we assume that the peak at  $m/z$   
403 135.0426 corresponds to the molecular ion and the peak at  $m/z$  136.0503 (more intense) to the  
404 protonated ion, with a mass gap between both of 1.0082 u, matching the mass of one hydrogen  
405 atom (1.0078 u). Then, we focus on the peaks observed at the nominal  $m/z$  137, to derive more  
406 information about the elements present in the molecule. We thus observe two adjacent peaks at this  
407 same nominal  $m/z$ : 137.0469 and 137.0537. The mass gap between both is 0.0068 u. Calculations  
408 based on their distance (in mass) from the protonated ion allow us to consider them both as  
409 isotopologues with the replacement in the molecular formula of the protonated ion of, respectively,  
410 one  $^{14}N$  by a  $^{15}N$  atom (first peak, with a mass gap of 0.9966 u) and one  $^{12}C$  by a  $^{13}C$  atom (second  
411 peak, with a mass gap of 1.0034 u). According to the nitrogen rule, the even  $m/z$  of the protonated  
412 ion implies an odd number of nitrogen atoms. At the nominal  $m/z$  138 we do not observe a clear  
413 signal, confirming the absence of sulphur and a low abundance of oxygen. Based on all these  
414 assumptions (a CHNO molecule, a protonated ion at a  $m/z$  close to 136.0503 u, the presence of an  
415 odd number of nitrogen atoms and oxygen in low abundance), 3 candidates are found compatible  
416 with a precision lower than 15 ppm on the exact mass attribution :  $C_6H_6N_3O^+$  (-0.9960 ppm),  $C_8H_8O_2^+$   
417 (8.8018 ppm) and  $C_4H_4N_6^+$  (-10.7940 ppm). The first possibility shows the lowest error. In addition,



418 the presence of an oxygen loss with mass gap calculations excludes the third attribution. To confirm  
419 our choice, we look at the  $C_6H_5N_3O$  molecule fragmentation pattern in the NIST database. We find  
420 that it is consistent with our spectrum (see Figure 7), mainly by the similar fragment ions at  $m/z$  107  
421 and 119. As for the comparison NIST/CosmOrbitrap made for adenine, all fragment ions are not  
422 comparable. More of them are detected on the NIST mass spectrum, obtained with a more energetic  
423 ionisation process. In this case, the  $m/z$  119 fragment ion is relevant enough to confirm our molecule  
424 selection.  
425



426  
427 *Figure 7: Mass spectrum of sample "A" (assumed to be HOBT) obtained with Lab-CosmOrbitrap (top panel) and mass*  
428 *spectrum of HOBT from NIST database (lower panel). Comparison between both fragmentation patterns.*

429  
430  
431 Indeed, the identification steps detailed in this section lead to consider the sample "A" as HOBT,  
432 standing for 1H-Benzotriazole,1-hydroxy-, which is a derivative of benzotriazole. The presence of the  
433 benzotriazole fragment ion is thus very specific and detected in the CosmOrbitrap mass spectrum, at  
434 nominal  $m/z$  119 (as well as in the NIST mass spectrum). The mass difference between the



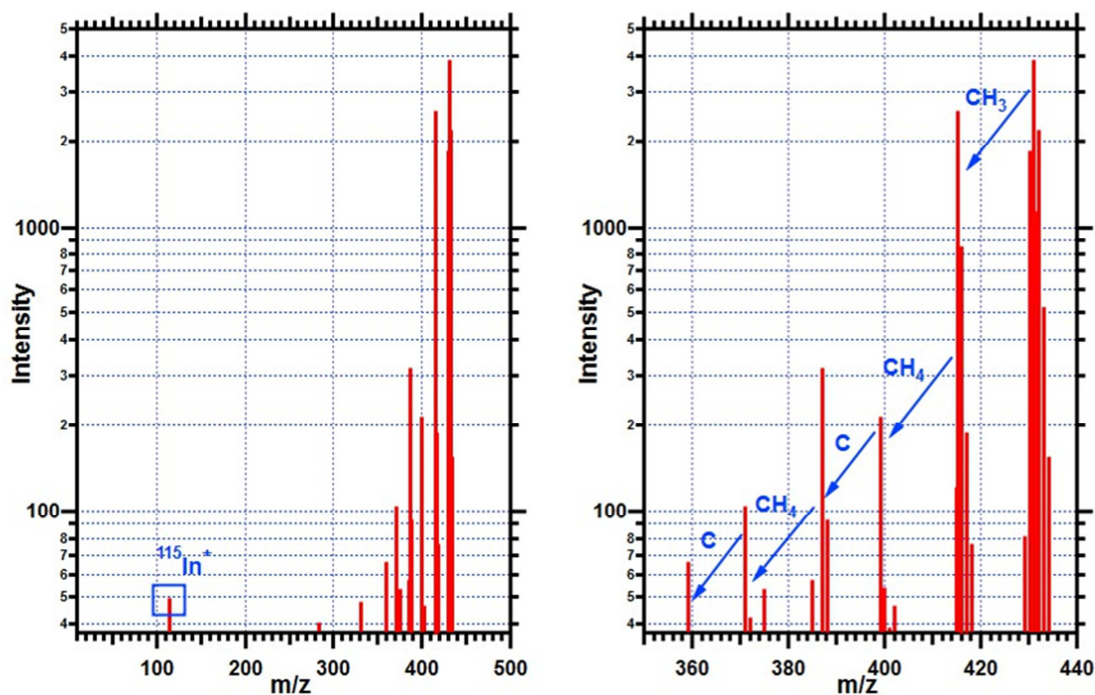
435 benzotriazole fragment ion and the molecular HOBt ion corresponds to the loss of an oxygen atom  
436 (15.9949 u). The MRP of the molecular ion at  $m/z$  135 is 123,540. This organic compound is an  
437 unstable molecule when on its anhydrous form, which could explain the observed variability  
438 between mass spectra. The heating from the laser beam at the surface of the sample in addition to  
439 the ultra-high vacuum surrounding the sample yield an outgassing of water molecules from the  
440 sample, causing the studied HOBt compound to become unstable. Peaks between  $m/z$  136 and 365  
441 are interpreted as recombination between fragments of HOBt and HOBt or fragments of HOBt with  
442 indium (as observed for the cluster [indium + HOBt]<sup>+</sup> at  $m/z$  250).

443

444           b) Identification of sample "B"

445

446 Using the same methodology, we obtain a mass spectrum for sample "B" with six specific and  
447 repeatable patterns from  $m/z$  350 to 440 (Figure 8). The indium peak at the nominal  $m/z$  115 is still  
448 visible (blue square in Figure 8, left spectrum), meaning the laser spot is at the edge of the sample  
449 deposit or the sample coverage at this point is thinner.



450

451 Figure 8: (Left) Overall mass spectrum of sample "B" from 10 to 550 m/z range (left), where the blue square indicates the  
 452 indium peak. (Right) Zoom on the six main patterns observed between 350 and 440 m/z range with the molecular formula of  
 453 the lost fragments.

454

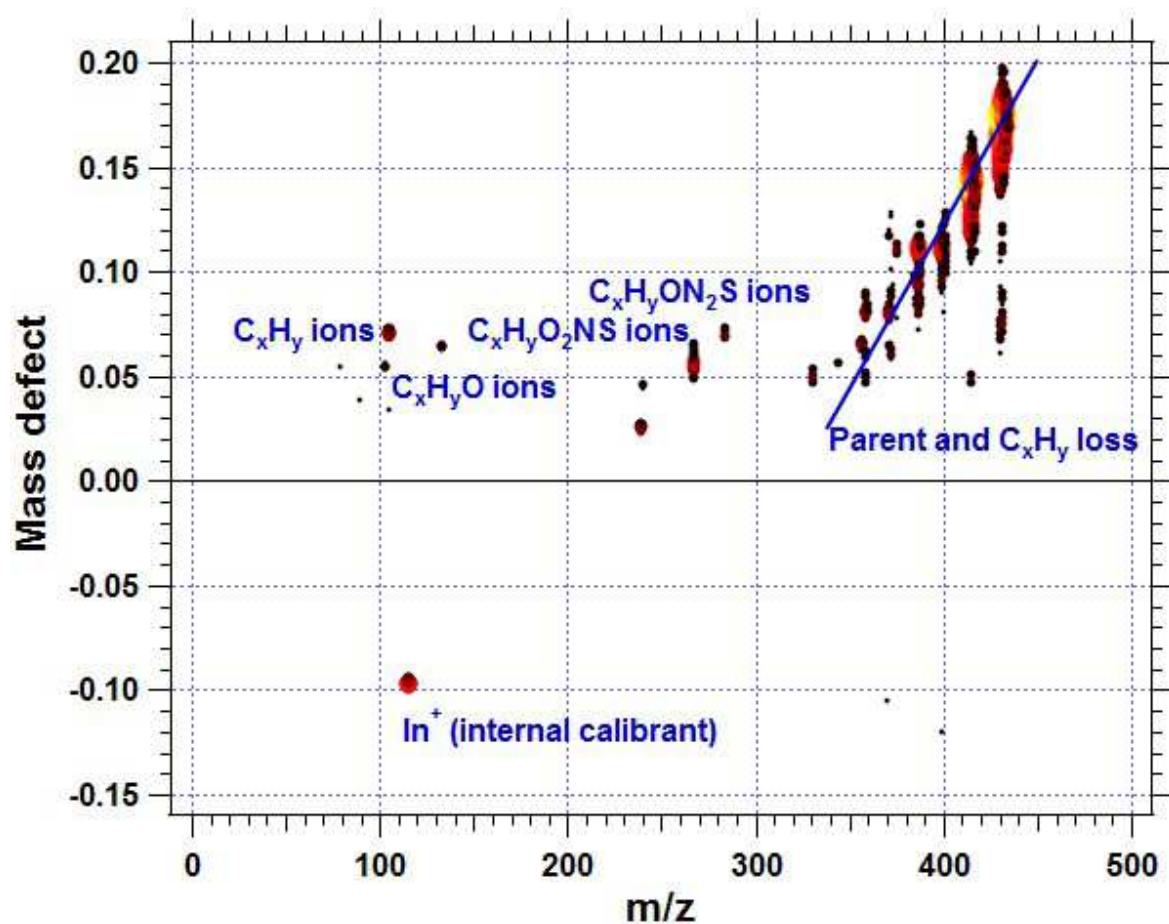
455

456 Within this mass range, the most intense peak is located at  $m/z$  431.1796. This observation is done  
 457 during several consecutive laser shots, showing a strong repeatability. We consider this peak as the  
 458 protonated ion of our molecule due to its mass difference of 1.0106 u, close to the mass of one  
 459 hydrogen atom (1.0078), with the peak observed one nominal mass lower. Based on this assumption,  
 460 the molecular ion should be the one located at  $m/z$  430.1690. Its MRP is about 69,219.

461 Then, we focus on peaks detected from  $m/z$  432 to 434. We interpret peaks at  $m/z$  432.1813 and  
 462 433.1832 as isotopologues of the protonated ion, showing the replacement of respectively one  $^{12}\text{C}$  by  
 463 one  $^{13}\text{C}$  and two  $^{12}\text{C}$  by two  $^{13}\text{C}$  in their molecular formula. The respective mass accuracy of these  
 464 attributions are -0.7 and -4.2 ppm. The peak detected at  $m/z$  434 should be an isotopologue with  
 465 three  $^{12}\text{C}$  replaced by three  $^{13}\text{C}$  in its molecular formula. The decreasing intensities of these three  
 466 peaks are consistent with the decreasing probabilities of carbon replacements in a given molecular

467 formula. The  $m/z$  434 isotopologue should be detected at  $m/z$  434.1884. We indeed observe this  
468 value, but this is not the peak maximum, due to the bad shape of this peak. The high intensity of the  
469 nominal  $m/z$  432 points to a large quantity of carbon atoms composing the molecular formula  
470 (around 30 carbon atoms to produce this signal intensity). At  $m/z$  433 we observe a twin peak. One  
471 has already been interpreted as two carbon isotopes replacement. The other one has to be  
472 identified. The mass difference between this peak at  $m/z$  433.1736 and the protonated ion is 1.9940  
473 u. This could match with the mass difference between two isotopes of several elements: chlorine  
474 (1.9970 u between  $^{35}\text{Cl}$  and  $^{37}\text{Cl}$ ), sulphur (1.9958 u between  $^{32}\text{S}$  and  $^{34}\text{S}$ ), nickel (1.9954 u between  
475  $^{58}\text{Ni}$  and  $^{60}\text{Ni}$ ) and iron (1.9983 u between  $^{56}\text{Fe}$  and  $^{58}\text{Fe}$ ). The theoretical abundances of  $^{37}\text{Cl}$  and  $^{60}\text{Ni}$   
476 do not match with the intensity of the observed peak (almost 25% for  $^{37}\text{Cl}$  and 26% for  $^{60}\text{Ni}$  against a  
477 mean of 10% for the experimental peak, based on several spectra), discarding these elements.  
478 Concerning iron, a peak should have been observed also at  $m/z$  432. Finally,  $^{34}\text{S}$  is the isotope  
479 presenting the best match in terms of mass difference and relative intensity from the protonated one  
480 (theoretical intensity of 4.5%). Based on the nitrogen rule, the odd mass of the protonated ion  
481 induces an even number of nitrogen elements in the molecule.

482



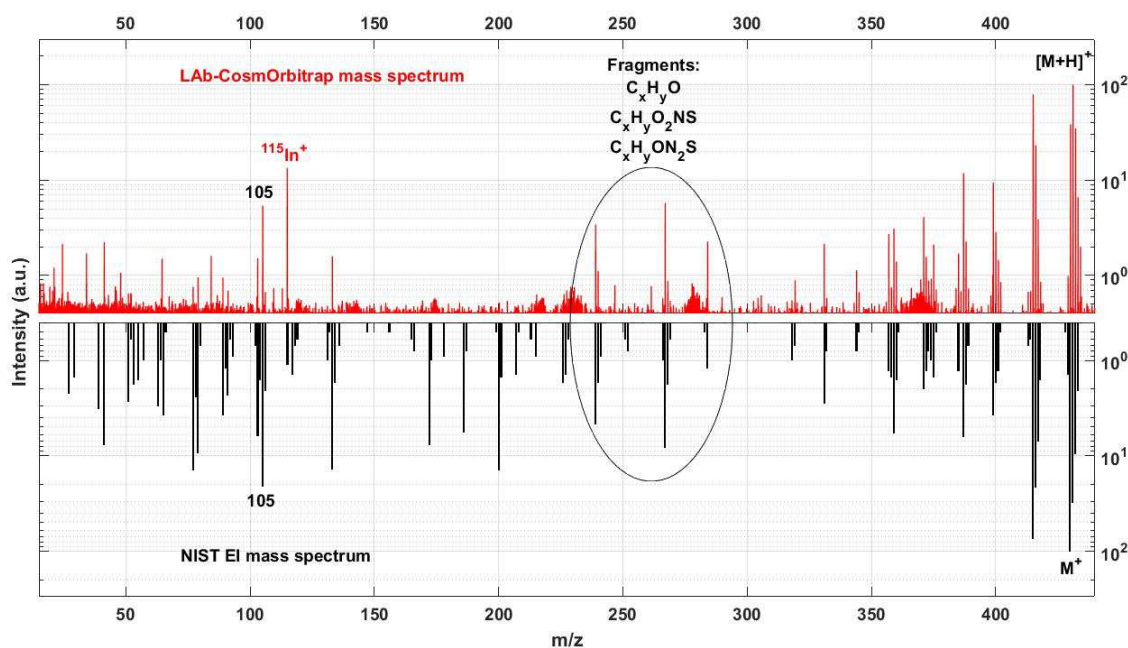
483  
 484 Figure 9: Mass Defect versus Exact Mass (MDvEM) diagram of « Sample B ». Similarly to the MDvEM diagram of sample “A”  
 485 (Figure 6), each ionic peak is represented as a dot corresponding to its mass defect as a function of its  $m/z$ , where, in  
 486 addition, the colour and the size of the dots are proportional to the log of their intensities in the mass spectra. As a  
 487 reminder, lighter colours (such as yellow then orange) corresponds to the most intense peaks and darker ones (dark red then  
 488 black) to the less intense peaks. The blue line represents the main trend line observed (losses of  $C_xH_y$  fragments). Other  
 489 groups identified are indicated on the diagram. The dot corresponding to the indium ion is the largest one presenting a  
 490 negative mass defect.

491  
 492 The specific patterns at nominal  $m/z$  415, 399, 387, 371 and 359 appear on the MDvEM diagram of  
 493 Figure 9. These points are following the same trend, as a signature of the loss of the same molecular  
 494 group, attributed in this case to specific losses of  $C_xH_y$  from the molecular ion and proving the  
 495 presence of abundant unsaturated chains in the structure of the molecule. These  $C_xH_y$  fragments  
 496 should be observed at lower masses. As we perform laser ablation, molecules are more and more

497 broken at each laser shot at the same location. By this way, fragmentation increases with the number  
498 of laser shots. In order to derive more information from the MDvEM diagram, we study another  
499 spectrum obtained a few laser shots following the first one studied. On this mass spectrum, we  
500 observe the same six patterns from  $m/z$  359 to 434 but also more fragment ions at lower intensities  
501 (as visible on Figure 9), coming from the fragmentation of species detected up to  $m/z$  434. At  
502 intermediate masses this diagram allows us to identify also the presence of oxygen by the  
503 observation of  $C_xH_yO$ ,  $C_xH_yO_2NS$  and  $C_xH_yON_2S$  ions signatures. These molecular formula are derived  
504 from assignments proposed by the Attributor software. Calculations based on the MDvEM diagram  
505 lead us to confirm some of them and particularly those given here. An example can be given based  
506 on the peaks observed at  $m/z$  105.0706 and 133.0651. Both values, in term of  $m/z$  and mass defect  
507 have to be consistent together to confirm which molecular group is lost or added between these two  
508 peaks. In this case, the molecular group should be CO. This is indeed corresponding (1) in term of  $m/z$   
509 (the experimental mass difference of 27.9945 u is very close to the theoretical one of 27.9949 u) and  
510 (2) in term of mass defect calculation where only the MD of oxygen is involved (as the MD of carbon  
511 is 0) with an experimental value of -0.0055 close the theoretical value of -0.0051.

512 Four candidates are found compatible within the precision of the spectrum:  $C_{26}H_{27}N_2O_2S^+$  (-2.2 ppm),  
513  $C_{23}H_{31}N_2O_2S_2^+$  (5.6 ppm),  $C_{20}H_{35}N_2O_2S_3^+$  (13.3 ppm),  $C_{20}H_{27}N_6O_3S^+$  (14.5 ppm).

514 The first candidate, presenting the best mass accuracy, is also the one that explains the high intensity  
515 observed at  $m/z$  432 (matching with a high number of carbon atoms). We decide to focus on this first  
516 molecule and to look at its fragmentation mass spectrum on the NIST database.



517  
 518 *Figure 10: Mass spectrum of sample "B" (assumed to be BBOT) obtained with LAB-CosmOrbitrap (top panel, in red) and*  
 519 *mass spectrum of BBOT from NIST database (low panel in reverse scale, in black). Comparison of fragmentation patterns*  
 520 *observed with these two techniques. Similarities are mainly observed in the  $m/z$  range 350 to 431, with some intense*  
 521 *fragment ions at nominal  $m/z$  105 and 267. In addition, the  $m/z$  range 230 to 300 allows the observation of  $C_xH_yO$ ,  $C_xH_yO_2NS$*   
 522 *and  $C_xH_yON_2S$  fragment ions, as described in the MDvEM diagram on the Figure 9.*

523  
 524 As for the identification process of sample A, we compare both mass spectra on the same figure  
 525 (Figure 10) with LAB-CosmOrbitrap mass spectrum on the top panel and NIST EI mass spectrum on  
 526 the lower panel. The match between both spectra is mostly visible between  $m/z$  350 and 431 but  
 527 some intense fragments at the nominal  $m/z$  105 and 267 are also observed. We select this molecule  
 528 and identify it as BBOT, standing for 2,5-Bis(5-tert-butyl-2-benzoxazolyl)thiophene at a theoretical  
 529 molecular and protonated  $m/z$  of, respectively, 430.1709 and 431.1787. The fragment ion at  $m/z$   
 530 267.057 can be interpreted as  $C_{15}H_{11}N_2OS$ , which corresponds to a loss of  $C_{11}H_{15}O$  consistent with the  
 531 peak observed at this  $m/z$  on the MDvEM diagram (Figure 9) and in the red mass spectrum (Figure 10  
 532 – inside the black-circle). Some discrepancies are also visible on this mass spectra comparison but  
 533 again, in this study we only focus on the main fragment ions produced by both techniques which  
 534 allow us to identify the species.

## 535 IV) Conclusion

536 Our blind analysis of the organic molecules A and B with the LAb-CosmOrbitrap prototype has led to  
537 the identification of respectively the two molecules HOBt (hydroxybenzotriazole,  $C_6H_5N_3O$ ) and BBOT  
538 (2,5-Bis(5-tert-butyl-benzoxazol-2-yl)thiophene,  $C_{26}H_{26}N_2O_2S$ ). Our attributions were afterwards  
539 positively confirmed by the JAXA HRMS team which had chosen and sent the samples.

540 Sample analysis and data treatment methodology require several steps. The process starts with a  
541 first visualisation of the full  $m/z$  range mass spectrum directly on the sample or at the edge of the  
542 sample and the metallic substrate, in order to add a specific feature by the production of cluster ions.  
543 This first step leads to the identification of the mass of the molecular ion. The high resolution of the  
544 spectrum enables attributions of the elements present in the molecule by calculation of mass  
545 spacing, within the precision of the spectra. To go deeper in the data treatment, the use of the mass  
546 defect versus exact mass (MDvEM) diagram allows to get information of possible repetitive patterns  
547 in the molecule to know more about the structure of the molecule and specific groups or atoms  
548 composing it. We can then infer the chemical formula of possible candidates. The comparison of the  
549 fragmentation patterns with the NIST EI (Electron Impact) spectra database finally confirms the  
550 selection of one molecule among the possible candidates.

551 This study shows the capability of the LAb-CosmOrbitrap instrument to identify unknown organic  
552 molecules. We also demonstrate that only a small amount of sample is needed to provide a good  
553 analysis. The instrument has an important potential for *in situ* chemical analysis of organic molecules  
554 during space exploration missions, as molecular identification capability is absolutely required for  
555 new instrumental developments. Precious clues are given here to anticipate what is needed for a  
556 space configuration. We show the crucial importance of the sample preparation and the nature of  
557 the sample-holder. Sample deposition on the surface of a metallic sample-holder offers the benefit of  
558 clusters formation. Moreover, the metallic sample-holder gives us a useful calibration mass point for  
559 the whole mass spectrum. Finally, following the work by the Briois et al, 2016 and to update  
560 analytical performances of the LAb-CosmOrbitrap on organics, we show the capability of our



561 instrumental configuration to reach a mass resolving power (MRP) of 69,219 at  $m/z$  430 and 123,540  
562 at  $m/z$  135. Mass accuracies better than 3 ppm (-0.9 ppm for HOBt and -2.2 ppm for BBOT) have  
563 been demonstrated. The LAb-CosmOrbitrap is thus a key instrument for future space missions and  
564 particularly for organic worlds, with analytical performances never reached in space to this date.  
565 However the study also points out some difficulties to be tackled in the future such as the variability  
566 resulting from the ionisation process chosen (laser ablation) but also from the intrinsic properties of  
567 the sample (UV absorption, ionisation potential). As a wide energy range can be applied on the  
568 sample, a specific Laser Ablation (and Desorption) CosmOrbitrap calibration mass spectra database  
569 would be relevant in order to get reference mass spectra at different energies of organic species  
570 presenting a potential exobiological interest. This database would allow a post data treatment of the  
571 spectra received from a spacecraft. In addition, a laser system with variable output energy should be  
572 set for a space configuration, in agreement with present laboratory configurations. On-board, data  
573 collection and mass spectra selection will highly depend on space mission parameters such as the  
574 mission duration, the scenario of the mission (flyby(s), encounter, escort etc.) and the targeted body.

575

576

577

578



579

580 **Acknowledgements**

581 L. S. thanks the CNES (Centre National d'Etudes Spatiales) and the Région Centre-Val de Loire for the  
582 funding of her PhD.

583 N.C. thanks the European Research Council for funding via the ERC PrimChem project (grant  
584 agreement No. 636829.)

585 We gratefully acknowledged CNES for funding the instrumental development of the CosmOrbitrap,  
586 the Labex Exploration Spatiale des Environnements Planétaires (ESEP), and the Région Centre-Val de  
587 Loire, Dr Titaina Gibert for lending us the Nd-Yag laser 266 nm used to perform all tests and the JAXA  
588 HRMS team for initiating this study.

589

## 590 References

- 591 Altwegg, K., Balsiger, H., Bar-Nun, A., Berthelier, J.-J., Bieler, A., Bochslers, P., Briois, C., Calmonte, U.,  
592 Combi, M.R., Cottin, H., De Keyser, J., Dhooghe, F., Fiethe, B., Fuselier, S.A., Gasc, S., Gombosi, T.I.,  
593 Hansen, K.C., Haessig, M., Jäckel, A., Kopp, E., Korth, A., Le Roy, L., Mall, U., Marty, B., Mousis, O.,  
594 Owen, T., Rème, H., Rubin, M., Sémon, T., Tzou, C.-Y., Hunter Waite, J., Wurz, P., 2016. Prebiotic  
595 chemicals—amino acid and phosphorus—in the coma of comet 67P/Churyumov-Gerasimenko. *Sci.*  
596 *Adv.* 2. <https://doi.org/10.1126/sciadv.1600285>
- 597 Balsiger, H., Altwegg, K., Bochslers, P., Eberhardt, P., Fischer, J., Graf, S., Jäckel, A., Kopp, E., Langer, U.,  
598 Mildner, M., Müller, J., Riesen, T., Rubin, M., Scherer, S., Wurz, P., Wüthrich, S., Arijs, E., Delanoye, S.,  
599 Keyser, J.D., Neefs, E., Nevejans, D., Rème, H., Aoustin, C., Mazelle, C., Médale, J.-L., Sauvaud, J.A.,  
600 Berthelier, J.-J., Bertaux, J.-L., Duvet, L., Illiano, J.-M., Fuselier, S.A., Ghielmetti, A.G., Magoncelli, T.,  
601 Shelley, E.G., Korth, A., Heerlein, K., Lauche, H., Livi, S., Loose, A., Mall, U., Wilken, B., Gliem, F.,  
602 Fiethe, B., Gombosi, T.I., Block, B., Carignan, G.R., Fisk, L.A., Waite, J.H., Young, D.T., Wollnik, H.,  
603 2007. Rosina – Rosetta Orbiter Spectrometer for Ion and Neutral Analysis. *Space Sci. Rev.* 128, 745–  
604 801. <https://doi.org/10.1007/s11214-006-8335-3>
- 605 Bhardwaj, C., Hanley, L., 2014. Ion sources for mass spectrometric identification and imaging of  
606 molecular species. *Nat. Prod. Rep.* 31, 756–767. <https://doi.org/10.1039/C3NP70094A>
- 607 Bieler, A., Altwegg, K., Balsiger, H., Bar-Nun, A., Berthelier, J.-J., Bochslers, P., Briois, C., Calmonte, U.,  
608 Combi, M., De Keyser, J., van Dishoeck, E.F., Fiethe, B., Fuselier, S.A., Gasc, S., Gombosi, T.I., Hansen,  
609 K.C., Hässig, M., Jäckel, A., Kopp, E., Korth, A., Le Roy, L., Mall, U., Maggiolo, R., Marty, B., Mousis, O.,  
610 Owen, T., Rème, H., Rubin, M., Sémon, T., Tzou, C.-Y., Waite, J.H., Walsh, C., Wurz, P., 2015.  
611 Abundant molecular oxygen in the coma of comet 67P/Churyumov–Gerasimenko. *Nature* 526, 678.
- 612 Bonnet, J.-Y., Thissen, R., Frisari, M., Vuitton, V., Quirico, É., Orthous-Daunay, F.-R., Dutuit, O., Le Roy,  
613 L., Fray, N., Cottin, H., Hörst, S.M., Yelle, R.V., 2013. Compositional and structural investigation of  
614 HCN polymer through high resolution mass spectrometry. *Detlef Schröder Meml. Issue* 354–355,  
615 193–203. <https://doi.org/10.1016/j.ijms.2013.06.015>
- 616 Briois, C., Thissen, R., Thirkell, L., Aradj, K., Bouabdellah, A., Boukrara, A., Carrasco, N., Chalumeau,  
617 G., Chapelon, O., Colin, F., Coll, P., Cottin, H., Engrand, C., Grand, N., Lebreton, J.-P., Orthous-Daunay,  
618 F.-R., Pennanech, C., Szopa, C., Vuitton, V., Zapf, P., Makarov, A., 2016. Orbitrap mass analyser for in  
619 situ characterisation of planetary environments: Performance evaluation of a laboratory prototype.  
620 *Planet. Space Sci.* 131, 33–45. <https://doi.org/10.1016/j.pss.2016.06.012>

- 621 Carrasco, N., Jomard, F., Vigneron, J., Etcheberry, A., Cernogora, G., 2016. Laboratory analogues  
622 simulating Titan's atmospheric aerosols: Compared chemical compositions of grains and thin films.  
623 *Planet. Space Sci.* 128, 52–57. <https://doi.org/10.1016/j.pss.2016.05.006>
- 624 Gautier, T., Schmitz-Afonso, I., Touboul, D., Szopa, C., Buch, A., Carrasco, N., 2016. Development of  
625 HPLC-Orbitrap method for identification of N-bearing molecules in complex organic material relevant  
626 to planetary environments. *Icarus* 275, 259–266. <https://doi.org/10.1016/j.icarus.2016.03.007>
- 627 Goesmann, F., Brinckerhoff, W.B., Raulin, F., Goetz, W., Danell, R.M., Getty, S.A., Siljeström, S.,  
628 Mißbach, H., Steininger, H., Arevalo, R.D., Buch, A., Freissinet, C., Grubisic, A., Meierhenrich, U.J.,  
629 Pinnick, V.T., Stalport, F., Szopa, C., Vago, J.L., Lindner, R., Schulte, M.D., Brucato, J.R., Glavin, D.P.,  
630 Grand, N., Li, X., van Amerom, F.H.W., 2017. The Mars Organic Molecule Analyzer (MOMA)  
631 Instrument: Characterization of Organic Material in Martian Sediments. *Astrobiology* 17, 655–685.  
632 <https://doi.org/10.1089/ast.2016.1551>
- 633 Grasset, O., Dougherty, M.K., Coustenis, A., Bunce, E.J., Erd, C., Titov, D., Blanc, M., Coates, A.,  
634 Drossart, P., Fletcher, L.N., Hussmann, H., Jaumann, R., Krupp, N., Lebreton, J.-P., Prieto-Ballesteros,  
635 O., Tortora, P., Tosi, F., Van Hoolst, T., 2013. JUPITER ICy moons Explorer (JUICE): An ESA mission to  
636 orbit Ganymede and to characterise the Jupiter system. *Planet. Space Sci.* 78, 1–21.  
637 <https://doi.org/10.1016/j.pss.2012.12.002>
- 638 Horneck, G., 1995. Exobiology, the study of the origin, evolution and distribution of life within the  
639 context of cosmic evolution: a review. *Exobiology* 43, 189–217. [https://doi.org/10.1016/0032-](https://doi.org/10.1016/0032-0633(94)00190-3)  
640 [0633\(94\)00190-3](https://doi.org/10.1016/0032-0633(94)00190-3)
- 641 Hörst, S.M., 2017. Titan's atmosphere and climate. *J. Geophys. Res. Planets* 122, 432–482.  
642 <https://doi.org/10.1002/2016JE005240>
- 643 Le Roy, L., Altwegg, K., Balsiger, H., Berthelier, J.-J., Bieler, A., Briois, C., Calmonte, U., Combi, M.R.,  
644 De Keyser, J., Dhooghe, F., Fiethe, B., Fuselier, S.A., Gasc, S., Gombosi, T.I., Hässig, M., Jäckel, A.,  
645 Rubin, M., Tzou, C.-Y., 2015. Inventory of the volatiles on comet 67P/Churyumov-Gerasimenko from  
646 Rosetta/ROSINA. *A&A* 583. <https://doi.org/10.1051/0004-6361/201526450>
- 647 Makarov, A., 2000. Electrostatic Axially Harmonic Orbital Trapping: A High-Performance Technique  
648 of Mass Analysis. *Anal. Chem.* 72, 1156–1162. <https://doi.org/10.1021/ac991131p>
- 649 Makarov, A., Denisov, E., Lange, O., 2009. Performance evaluation of a high-field orbitrap mass  
650 analyzer. *J. Am. Soc. Mass Spectrom.* 20, 1391–1396. <https://doi.org/10.1016/j.jasms.2009.01.005>

- 651 Murray Kermit K., Boyd Robert K., Eberlin Marcos N., Langley G. John, Li Liang, Naito Yasuhide, 2013.  
652 Definitions of terms relating to mass spectrometry (IUPAC Recommendations 2013). *Pure Appl.*  
653 *Chem.* 85, 1515. <https://doi.org/10.1351/PAC-REC-06-04-06>
- 654 Orthous-Daunay, F.-R., Quirico, E., Beck, P., Brissaud, O., Dartois, E., Pino, T., Schmitt, B., 2013. Mid-  
655 infrared study of the molecular structure variability of insoluble organic matter from primitive  
656 chondrites. *Icarus* 223, 534–543. <https://doi.org/10.1016/j.icarus.2013.01.003>
- 657 Pernot, P., Carrasco, N., Thissen, R., Schmitz-Afonso, I., 2010. Tholinomics—Chemical Analysis of  
658 Nitrogen-Rich Polymers. *Anal. Chem.* 82, 1371–1380. <https://doi.org/10.1021/ac902458q>
- 659 Perry, R.H., Cooks, R.G., Noll, R.J., 2008. Orbitrap mass spectrometry: Instrumentation, ion motion  
660 and applications. *Mass Spectrom. Rev.* 27, 661–699. <https://doi.org/10.1002/mas.20186>
- 661 Phillips, C., Pappalardo, R., 2014. Europa Clipper Mission Concept: Exploring Jupiter’s Ocean Moon.  
662 <https://doi.org/10.1002/2014EO200002>
- 663 Rubin, M., Altwegg, K., Balsiger, H., Bar-Nun, A., Berthelier, J.-J., Bieler, A., Bochslers, P., Briois, C.,  
664 Calmonte, U., Combi, M., De Keyser, J., Dhooghe, F., Eberhardt, P., Fiethe, B., Fuselier, S.A., Gasc, S.,  
665 Gombosi, T.I., Hansen, K.C., Hässig, M., Jäckel, A., Kopp, E., Korth, A., Le Roy, L., Mall, U., Marty, B.,  
666 Mousis, O., Owen, T., Rème, H., Sémon, T., Tzou, C.-Y., Waite, J.H., Wurz, P., 2015. Molecular  
667 nitrogen in comet 67P/Churyumov-Gerasimenko indicates a low formation temperature. *Science*  
668 348, 232. <https://doi.org/10.1126/science.aaa6100>
- 669 Waite, J.H., Glein, C.R., Perryman, R.S., Teolis, B.D., Magee, B.A., Miller, G., Grimes, J., Perry, M.E.,  
670 Miller, K.E., Bouquet, A., Lunine, J.I., Brockwell, T., Bolton, S.J., 2017. Cassini finds molecular  
671 hydrogen in the Enceladus plume: Evidence for hydrothermal processes. *Science* 356, 155.  
672 <https://doi.org/10.1126/science.aai8703>
- 673 Waite, J.H., Lewis, W.S., Kasprzak, W.T., Anicich, V.G., Block, B.P., Cravens, T.E., Fletcher, G.G., Ip, W.-  
674 H., Luhmann, J.G., Mcnutt, R.L., Niemann, H.B., Parejko, J.K., Richards, J.E., Thorpe, R.L., Walter, E.M.,  
675 Yelle, R.V., 2004. The Cassini Ion and Neutral Mass Spectrometer (INMS) Investigation. *Space Sci. Rev.*  
676 114, 113–231. <https://doi.org/10.1007/s11214-004-1408-2>
- 677 Waite, J.H., Young, D.T., Cravens, T.E., Coates, A.J., Crary, F.J., Magee, B., Westlake, J., 2007. The  
678 Process of Tholin Formation in Titan’s Upper Atmosphere. *Science* 316, 870.  
679 <https://doi.org/10.1126/science.1139727>
- 680 Young, D.T., Berthelier, J.J., Blanc, M., Burch, J.L., Coates, A.J., Goldstein, R., Grande, M., Hill, T.W.,  
681 Johnson, R.E., Kelha, V., McComas, D.J., Sittler, E.C., Svenes, K.R., Szegö, K., Tanskanen, P., Ahola, K.,

682 Anderson, D., Bakshi, S., Baragiola, R.A., Barraclough, B.L., Black, R.K., Bolton, S., Booker, T., Bowman,  
683 R., Casey, P., Crary, F.J., Delapp, D., Dirks, G., Eaker, N., Funsten, H., Furman, J.D., Gosling, J.T.,  
684 Hannula, H., Holmlund, C., Huomo, H., Illiano, J.M., Jensen, P., Johnson, M.A., Linder, D.R., Luntama,  
685 T., Maurice, S., McCabe, K.P., Mursula, K., Narheim, B.T., Nordholt, J.E., Preece, A., Rudzki, J.,  
686 Ruitberg, A., Smith, K., Szalai, S., Thomsen, M.F., Viherkanto, K., Vilppola, J., Vollmer, T., Wahl, T.E.,  
687 Wüest, M., Ylikorpi, T., Zinsmeyer, C., 2004. Cassini Plasma Spectrometer Investigation. Space Sci.  
688 Rev. 114, 1–112. <https://doi.org/10.1007/s11214-004-1406-4>

689 **Website source:**

690 Attributor software of HRMS analysis at <https://frobsite.wordpress.com/reasearch/attributor/>, last  
691 access April 2018